ISSN (Print) 1226-1750
ISSN (Online) 2233-6656
Journal of Magnetics 26(1), 19-24 (2021) https://doi.org/10.4283/JMAG.2021.26.1.019

Tuning Structural, Magnetic and Photocatalytic Properties of Bi-Substituted Cobalt Ferrite Nanoparticles

Didik Eko Saputro, Retna Arilasita, Utari, and Budi Purnama*

Department of Physics, Faculty of Mathematics and Natural Sciences, Universitas Sebelas Maret, Jl. Ir. Sutami 36 A Kentingan Surakarta 57126, Indonesia

(Received 9 December 2020, Received in final form 19 March 2021, Accepted 22 March 2021)

We modified synthesis i.e. coprecipitation and centrifuge-precipitation procedures as well as substituted bismuth cation for tuning the structural, magnetic, and photocatalytic properties. The product was annealed at 1000 °C for 5 h. The results of XRD analysis show the single phase of high-purity magnetic nanoparticles is obtained experimentally. The vibrating sample magnetometer results indicate that saturated magnetization decreased slightly in the centrifuge-precipitation procedure compared to coprecipitation. Finally, the photocatalytic properties also change with the modification procedure as well as substituted bismuth cation. The highest reduction of 78.1 % in methylene blue under ultraviolet radiation indicates that nanoparticles in cobalt ferrite-based nanoparticles materials have the potential to function as photocatalyst materials.

Keywords : cobalt ferrite, nanoparticles, coprecipitation, centrifuge-precipitation, photocatalytic

1. Introduction

Recently, the substituted nonmagnetic material Bi^{3+} in inverse spinel $CoFe_2O_4$ nanoparticles has received significant attention. The metal cation Co^{2+} only occupies octahedral sites whereas the metal cation of Bi^{3+} and Fe^{3+} may occupy both octahedral and tetrahedral sites. The Bi^{3+} replaces Fe^{3+} in the octahedral sites modifying their structural properties, electrical properties as well as the magnetic characteristic [1-5]. The addition of bismuth to cobalt ferrite nanoparticles modifies the electronic structure, thereby creating potential applications in information storage technology [1-4] and also as photocatalyst [5-8].

The addition of Bi^{3+} ions to cobalt ferrite was reported to reduce the crystallite size. The presence of nonmagnetic bismuth ions also decreases the magnetization saturation [1, 2, 5]. The functional photocatalyst bismuth cobalt ferrite nanoparticles are interesting due to their potential application in reducing environmental pollution. A bismuth cobalt ferrite photocatalyst has been reported to reduces Congo red dye [6, 7], Evan blue [8], and phenol [5]. Different synthesis methods also affect the photocatalytic performance of bismuth cobalt ferrite nanoparticles [5]. Moreover, different of cation substituted cobalt ferrite nanoparticles also contribute to photocatalytic performance [6, 9-14].

Many methods have been developed for synthesis of bismuth cobalt ferrite nanoparticles during the last year, including the glycine nitrate synthesis method [1], solution combustion method [5, 6], sol-gel auto combustion [15], and the coprecipitation method [5, 16]. Among these procedures, the coprecipitation method is popular due to its low cost, simplicity, nontoxic precursors, industrial scale yields, and quick process.

In this study, we modified physical properties of the cobalt ferrite bismuth nano particles with such kind additional step in coprecipitation procedure and substituted bismuth cation. Therefore, the modified physical properties of the samples were examined i.e., structural properties by using x-ray diffractometer (XRD) and Fourier Transform Infra-Red (FTIR) as well as magnetics properties by using vibrating samples magnetometer (VSM). Finally, the photocatalytic performance was evaluated in methylene blue with additional of the obtained nanoparticle magnetic samples under illuminated ultra-violet light.

2. Experimental Methods

As mentioned previously, cobalt-ferrite-based nanoparticles

*Corresponding author: Tel: +62-271-669017
Fax: +62-271-669017, e-mail: bpurnama@mipa.uns.ac.id

was synthesized using the coprecipitation method [17, 18]. Stoichiometric quantities of high-purity $Co(NO_3)_2{\cdot}6H_2O$, $Fe(NO_3)_3{\cdot}9H_2O$, and $Bi(NO_3)_3{\cdot}5H_2O$ were dissolved in 200 ml of aqua bides while stirring at 250 rpm for 10 minutes until a homogenous solution was obtained. A 100-ml 4.8 M NaOH solution was then added dropwise to the obtained solution. During titration, the NaOH solution was stirred at 1000 rpm, and the temperature was maintained at 95 °C. The solution was then stirred continually for two hours. In order to modify the physical property, the obtained samples separately two-part, first cobalt ferrite and cobalt ferrite bismuth nanoparticles follow the centrifuge treatments (namely centrifuge coprecipitation) and second aging procedure for 24 hours (coprecipitation). Then, the precipitate was washed repeatedly with distilled water to obtain a clean precipitate product. To remove the residual water, the product was dried overnight in an oven at 100 °C. After annealed 1000 °C for 5 hours, samples were evaluated the crystalline structures by using the x-ray diffraction using a Bruker D8 Advance system. The bonding properties of the magnetic nanoparticles was observed using FTIR (Shimadzu IR Prestige 21). Their magnetic properties were evaluated using VSM (vibrating sample magnetometer) at room temperature. Finally, a methylene blue (10 ppm) solution was used to evaluate the photocatalysts under UV-Vis radiation for five minutes duration time with 10 mg addition modified cobalt ferrite-based materials.

3. Results and Discussions

Figure 1 shows the XRD patterns of cobalt ferrite ($CoFe_2O_4$) and bismuth substituted cobalt ferrite ($CoFe_{1.9}Bi_{0.1}O_4$) samples obtained by the coprecipitation and centrifuge-precipitation methods. Note that all diffraction peaks correspond to the (111), (220), (311), (222), (400), (422), (511), and (440) planes correspond to 2θ angles of the data on International Centre for Diffraction Data (ICDD) no 22-1086. No other peaks were observed that confirmed the presence of single-phase inverse spinel face center cubic (fcc) structure. Angles (2θ) of the highest peak (311) of the $CoFe_2O_4$ and $CoFe_{1.9}Bi_{0.1}O_4$ samples as obtained by the coprecipitation and centrifuge-precipitation methods are listed in Table 1.

Table 1 shows that the angles (2θ) of the highest peak of the bismuth substituted cobalt ferrite nanoparticles

Table 1. Angles (2θ) of highest peak (311) of $CoFe_2O_4$ and $CoFe_{1.9}Bi_{0.1}O_4$ samples.

Method	Angles (2θ)
Coprecipitation	
$CoFe_2O_4$	35.49°
$CoFe_{1.9}Bi_{0.1}O_4$	35.45°
Centrifuge-precipitation	
$CoFe_2O_4$	35.53°
$CoFe_{1.9}Bi_{0.1}O_4$	35.43°

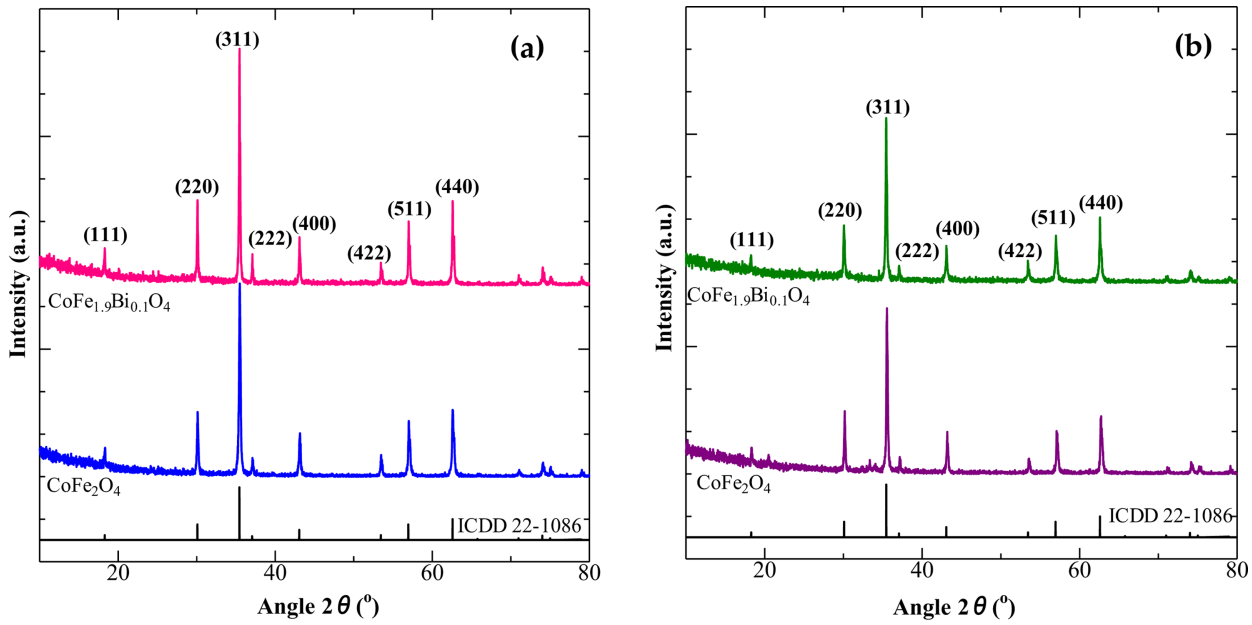

Fig. 1. (Color online) XRD patterns of $CoFe_2O_4$ and $CoFe_{1.9}Bi_{0.1}O_4$ nanoparticles synthesized at 95 °C by the (a) coprecipitation and (b) centrifuge-precipitation methods following annealing at 1000 °C for five hours under atmospheric air conditions.

slightly shift to the left by 0.04° and 0.10° compared to cobalt ferrite nanoparticles for both the samples obtained by the coprecipitation, and centrifuge-precipitation methods, respectively. The 2θ angle shift in the presence of bismuth ions in a sample of the magnetic nanoparticles is consistent with results reported by Gore *et al.* 2017 [15]. Shifting the peak angle of the XRD also shows the evolution of crystallites [1, 19]. This indicates a change in the microstructure; however, the original structure of the cobalt ferrite remained unchanged in the presence of bismuth ions. To examine such changes in the sample's microstructure in greater detail, crystalline parameters, i.e., crystallite size D, lattice parameter a, density ρ, and lattice strain ε, were calculated. The crystallite size D was calculated as follows [20].

$$D = \frac{0.9\lambda}{\beta\cos\theta} \tag{1}$$

Here, λ is the XRD wavelength (source Cu K_α λ = 0.154 nm), β is the full width at half maximum (FWHM) of the highest peak in the orientation Miller Indices *hkl* (311), and θ is the angle corresponding to the highest peak of the XRD patterns.

Lattice parameter a was calculated as follows [21].

$$a = \frac{\lambda}{2\sin\theta}\sqrt{h^2 + k^2 + k^2} \tag{2}$$

The samples' density was calculated as follows.

$$d_x = \frac{ZM}{N_A a^3} \tag{3}$$

Here, Z is the number of molecules per unit cell, M is molecular weight, and NA is Avogadro's number.

The strain of the samples was calculated using the Hall-Williamson formula [20] as follows.

$$\varepsilon = \frac{\beta_{hkl}}{4\tan\theta} \tag{4}$$

Here, ε is strain, and β_{hkl} is the FWHM of the highest peak in the XRD pattern.

The calculated crystal parameters are listed in Table 2.

The crystallite size of cobalt ferrite with substitution of bismuth ions increased from 38.60 nm to 49.63 (an increase of 28.57 % (= 49.63-38.60/38.60)) with the Table 2. Similarly, for the centrifuge-precipitation method, the crystallite size increased by 13.41 nm (53.09 nm-39.68 nm), which is an increase of 33.79 % (53.09-39.68/39.68). This is consistent with the observation results obtained by Kiran and Sumathi [5]. The increased crystallite size obtained with the centrifuge-precipitation method indicates that the centrifuge energy seem contribute to the substitution of bismuth ions such that the density of cobalt ferrite nanoparticles is reduced when bismuth (Bi^{3+}) ions substitute the ferrite (Fe^{3+}) ions in the cobalt ferrite structure. Consequently, the strains of both samples obtain by the coprecipitation and centrifuge-precipitation methods decreased. Modification of the lattice crystalline parameters and crystallite size contribute to the stretching vibration of Fe^{3+}–O^{2-}, which is reflected as a shift in the band positions of the FTIR absorption curve. It mean that the substitution of bismuth ions in cobalt ferrite nanoparticles affects some structural changes, as mentioned in the previous paragraph, and these structural changes are caused by integration of metal ions, which affect the lattice vibration.

Figures 2 shows the FTIR curve of the $CoFe_2O_4$ and $CoFe_{1.9}Bi_{0.1}O_4$ nanoparticles. Note that the FTIR spectra data for the samples were recorded from 350 to 4000 cm^{-1}. The absorption band (tetrahedral band) is appropriate to the intrinsic stretching vibrations of metal iron and oxygen bonding (Fe-O) in wavenumber for around k_1 = 590 cm^{-1} which explains the spinel ferrite structure formation. Thus, the second characteristics of this absorption band (octahedral band) are at the wavenumber k_2 ~390 cm^{-1} because that is a reasonable fit to the cobalt ferrite sample, i.e., approximately 400 cm^{-1} [5, 23]. It is safe to conclude that there is no new metal-oxide bonding regarding to substituted Bismuth in cobalt ferrite nano particles.

The force constant at the tetrahedral and octahedral

Table 2. Crystal parameters of $CoFe_2O_4$ and $CoFe_{1.9}Bi_{0.1}O_4$ nanoparticles synthesized at 95 °C by coprecipitation and centrifuge-precipitation methods.

	Crystallite size (nm)	Lattice parameter (Å)	Density (d_x/cm^3)	Lattice strain (× 10^{-3})
		Coprecipitation		
$CoFe_2O_4$	38.60	8.38	5.29	2.94
$CoFe_{1.9}Bi_{0.1}O_4$	49.63	8.38	5.28	2.29
		Centrifuge-precipitation		
$CoFe_2O_4$	39.68	8.36	5.32	2.86
$CoFe_{1.9}Bi_{0.1}O_4$	53.09	8.39	5.28	2.14

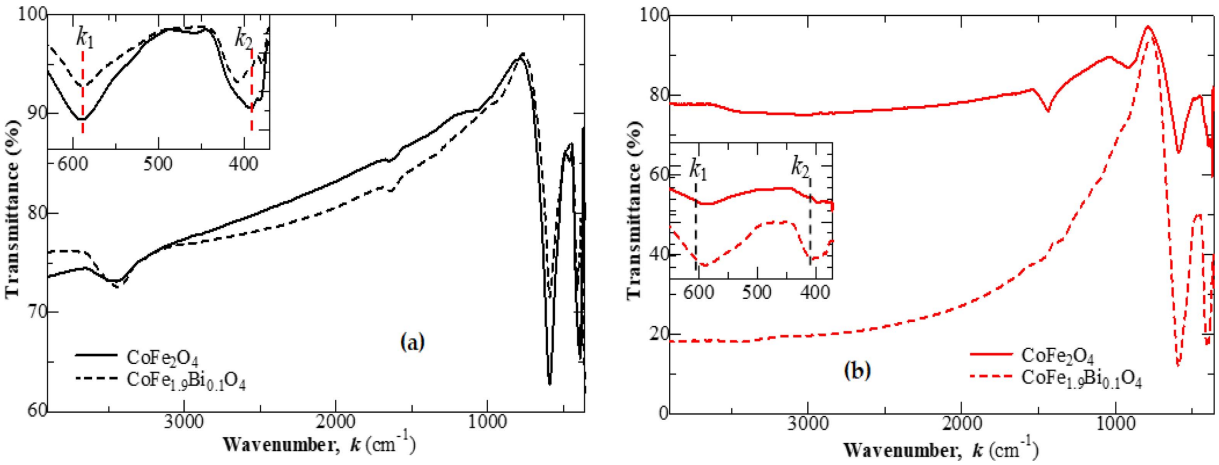

Fig. 2. (Color online) FTIR curves of $CoFe_2O_4$ and $CoFe_{1.9}Bi_{0.1}O_4$ nanoparticles synthesized at 95 °C by (a) coprecipitation and (b) centrifuge-precipitation methods following annealing at 1000 °C for five hours under atmospheric air conditions.

sites for the $CoFe_2O_4$ and $CoFe_{1.9}Bi_{0.1}O_4$ nanoparticles are shown in Table 2. The force constant for the tetrahedral (k_t) and octahedral (k_o) sites were calculated as follows [22].

$$k_t = 7.62 \times M_1 \times k_1^2 \times 10^{-7} \frac{N}{m} \quad (5)$$

$$k_o = 10.62 \times \frac{M_2}{2} \times k_2^2 \times 10^{-7} \frac{N}{m} \quad (6)$$

Here, M_1 is the molecular weight of the cations for the $CoFe_2O_4$ and $CoFe_{1.9}Bi_{0.1}O_4$ nanoparticles in the tetrahedral-site and M_2 in the octahedral-site, respectively.

The force constant calculation at the tetrahedral and octahedral sites indicates change with the different pre-

Table 3. Wavenumber, force constant at tetrahedral (k_t) and octahedral (k_o) of $CoFe_2O_4$ and $CoFe_{1.9}Bi_{0.1}O_4$ nanoparticles synthesized at 95 °C by coprecipitation and centrifuge-precipitation methods.

Method	k_1 (cm^{-1})	k_2 (cm^{-1})	k_t (N/m)	k_o (N/m)	Average (N/m)
		Coprecipitation			
$CoFe_2O_4$	590.24	389.64	14.83	9.25	12.04
$CoFe_{1.9}Bi_{0.1}O_4$	588.31	406.03	14.73	10.05	12.39
		Centrifuge-precipitation			
$CoFe_2O_4$	586.39	382.89	14.63	8.94	11.78
$CoFe_{1.9}Bi_{0.1}O_4$	590.24	393.50	14.83	9.44	12.13

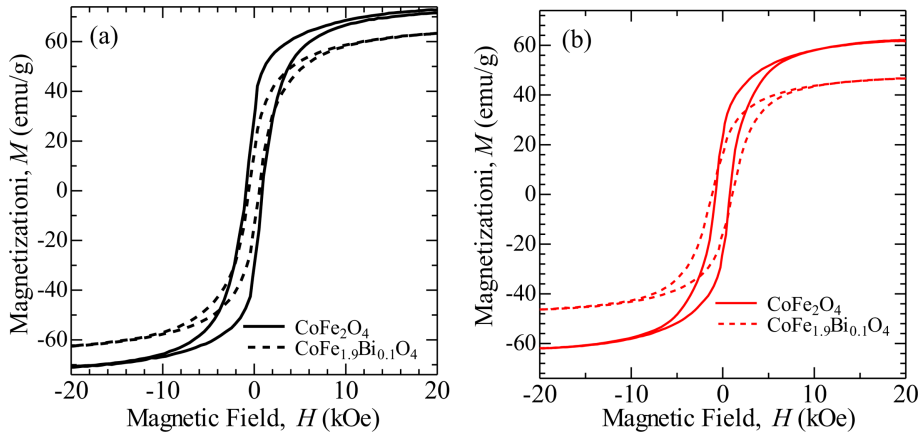

Fig. 3. (Color online) Hysteresis curves of $CoFe_2O_4$ and $CoFe_{1.9}Bi_{0.1}O_4$ nanoparticles synthesized by (a) coprecipitation and (b) centrifuge-precipitation methods following post annealing treatment at 1000 °C for five hours.

Table 4. Remanence magnetization, magnetic saturation, and coercive field of $CoFe_2O_4$ and $CoFe_{1.9}Bi_{0.1}O_4$ nanoparticles synthesized at 95 °C by coprecipitation and centrifuge-precipitation methods.

Method	Mr (emu/g)	Ms (emu/g)	Hc (kOe)	Mr/Ms
		Coprecipitation		
$CoFe_2O_4$	33.89	71.93	0.962	0.471
$CoFe_{1.9}Bi_{0.1}O_4$	18.31	62.97	0.585	0.291
		Centrifuge-precipitation		
$CoFe_2O_4$	23.54	62.03	0.693	0.379
$CoFe_{1.9}Bi_{0.1}O_4$	15.98	46.77	1.04	0.342

paration procedure. However, the total force constant, i.e., the average force constant at the octahedral and tetrahedral sites, typically demonstrates the same dependence of bismuth content for both the coprecipitation and centrifuge-precipitation procedures. Here, the average force constant increased from 12.04 to 12.30 N/m or 2.15% (= 12.30-12.04/12.04) for the coprecipitation method. Similarly, for the centrifuge-precipitation method, the average force constant modification was 0.35 N/m or 2.97% (= 12.13-11.78/11.78). The change in average force constant can be attributed to the change in crystallite size. Thus, the change in the structural characteristic modified both the magnetic and photocatalytic properties.

Figure 3 shows the magnetization curve of the cobalt ferrite and bismuth substituted cobalt ferrite nanoparticles obtained by the coprecipitation and centrifuge-precipitation methods. As can be seen in Fig. 3, the hysteresis curve of the coprecipitation samples reached magnetization saturation when the magnetic field exceeded 15 kOe. The centrifuge-precipitation samples required a magnetic field of approximately 10 kOe to achieve magnetization saturation. The saturation magnetization of the coprecipitation samples was greater than that of the centrifuge coprecipitation samples. The magnetic quantities results revealed from the hysteresis curve are presented in Table 3.

For the coprecipitation method, the magnetization saturation (M_S) the cobalt ferrite and bismuth substituted cobalt ferrite samples was 71.93 emu/g and 62.97 emu/g, respectively. With centrifuge-precipitation, the M_S values of 62.03 emu/g and 46.77 emu/g were obtained for the cobalt ferrite and bismuth substituted cobalt ferrite nanoparticles, respectively. These results are consistent with those reported by Panda *et al.* [19]. The decreased saturation magnetization could be explained by the magnetic dilution of the ferrite system via substitution of a nonmagnetic ion. The squareness of the hysteresis curve (M_r/M_S) appears to be consistent with M_S. M_r/M_S appears to be consistent with the rise in M_S, which indicates that crystalline magnetic anisotropy contributes to M_S.

For the coercive field (H_c), in the coprecipitation method, the H_c was 0.962 kOe for cobalt ferrite and 0.585 kOe for bismuth substituted cobalt ferrite nanoparticles. Here, the crystalline magnetic anisotropy should contribute to reducing the H_c. Thus, with centrifuge coprecipitation, H_c increased from 0.693 Oe to 1.04 kOe for the cobalt ferrite and bismuth substituted cobalt ferrite nanoparticles, respectively. Here, the modification of the crystallite size should contribute to the increased H_c.

The photocatalytic properties of the $CoFe_2O_4$ and

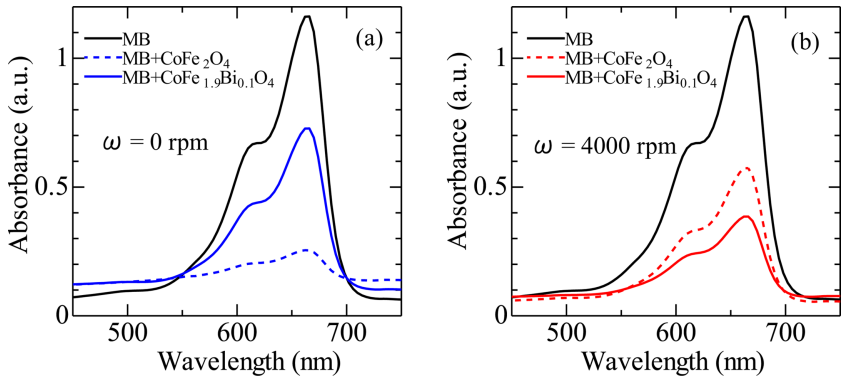

Fig. 4. Photocatalytic properties of $CoFe_2O_4$ and $CoFe_{1.9}Bi_{0.1}O_4$ nanoparticles synthesized by (a) coprecipitation and (b) centrifuge-precipitation methods following post annealing treatment at 1000 °C for five hours.

$CoFe_{1.9}Bi_{0.1}O_4$ nanoparticles synthesized by the coprecipitation and centrifuge-precipitation methods under degradation of methylene blue were evaluated under ultraviolet light for five minutes, as shown in Fig. 4. With the coprecipitation method, the efficiency removes methylene blue of 78.1 % and 37.4 % were obtained for $CoFe_2O_4$ and $CoFe_{1.9}Bi_{0.1}O_4$ nanoparticles, respectively. Here, the change in crystallite size should contribute the lowering efficiency photocatalytic properties. As discussed previously, crystallite sizes increased due to the addition of bismuth content. With the centrifuge-precipitation method, reductions of 50.6 % and 66.8 % were obtained for the $CoFe_2O_4$ and $CoFe_{1.9}Bi_{0.1}O_4$ nanoparticles, respectively. In the case of cobalt ferrite nano particle, the centrifuge-coprecipitation procedure causes the size of the crystallite to increase, so that the photocatalyst efficiency decreases by 35.2 % (= 78.1-50.6/78.1). While for the case of bismuth substitution of cobalt ferrite, the increase of the crystallite size increased photocatalyst efficiency from 34.4 % to 66.8 % or increased by 94.19 %. Here, the increase in the crystallite size of bismuth cobalt ferrite nanoparticles does not reduce the efficiency of photocatalysts as in the case of cobalt ferrite nano particles. Bismuth substituted cobalt ferrite nano particles define the photocatalytic absorption procedure which does not only depend on the particle size.

4. Conclusions

This paper has discussed changes to the structural, magnetic, and photocatalytic properties of cobalt-ferrite-based nanoparticles obtained by coprecipitation and centrifuge-precipitation methods as well as bismuth substituted cation. High-purity cobalt-ferrite-based nanoparticles were obtained experimentally, and XRD analysis results demonstrate that the centrifuge-precipitation samples had lower intensity than the coprecipitation samples. The vibrating sample magnetometer results indicate that the saturated magnetization decreased slightly with the centrifuge-precipitation method compared to the coprecipitation method. Finally, the highest reduction of 78.1 % in methylene blue under ultraviolet radiation indicates that cobalt ferrite-based nanoparticle materials have the potential to function as photocatalytic materials.

Acknowledgements

This research was funded by Penelitian Mandatory, DIPA PNBP Universitas Sebelas Maret, Kementerian Riset, Teknologi, dan Pendidikan Tinggi, The Republic of Indonesia, contract No. 516/UN27.21/PP/2019.

References

[1] N. S. Kumar and K. V. Kumar, Soft Nanoscience Letters **06**, 37 (2016).
[2] K. L. Routray, D. Sanyal, and D. Behera, J. Appl. Phys. **122**, 224104 (2017).
[3] S. Kapoor, A. Goyal, S. Bansal, and S. Singhal, New J. Chem. **42**, 14965 (2018).
[4] K. L. Routray, D. Sanyal, and D. Bahera, Mater. Res. Bull. **110**, 126 (2019).
[5] V. S. Kiran and S. Sumanthi, J. Magn. Magn. Mater. **421**, 113 (2017).
[6] V. S. Kirankumar and S. Sumanthi, J. Mater. Sci. **29**, 8738 (2018).
[7] M. A. Iqbal, S. I. Ali, F. Amin, A. Tariq, and M. Z. Iqbal, ACS Omega **4**, 8661 (2019).
[8] A. Paliwal, R. Ameta, and S. C. Ameta, European Chem. Bull. **6**, 120 (2017).
[9] S. Sumathi and V. Lakshmipriya, J. Mater. Sci. **28**, 2795 (2017).
[10] A. Samavati and A. F. Ismail, Particuology **30**, 158 (2017).
[11] P. Mahajan, A. Sharma, B. Kaur, N. Goyal, and S. Gautam, Vacuum **161**, 389 (2019).
[12] V. S. Kirankumar and S. Sumathi, Env. Sci. Poll. Res. **26**, 19189 (2019).
[13] M. M. Naik, H. S. B. Naik, G. Nagaraju, and M. Vinuth, Nano Str. Nano Obj. **19**, 100322 (2019).
[14] M. Sun, X. Han, and S. Chen, Mater. Sci. Semi. Proc. **91**, 367 (2019).
[15] S. K. Gore, S. S. Jadhav, V. V. Jadhav, S. M. Patage, M. Naushad, R. S. Mane, and K. H. Kim, Sci. Rep. **7**, 1 (2017).
[16] D. E. Saputro, Utari, and B. Purnama, J. Phys: Conf. Series **1153**, 012057 (2019).
[17] B. Purnama, R. Rahmawati, and A. T. Wijaya, J. Magn. **20**, 207 (2015).
[18] D. E. Saputro, U. Utari, and B. Purnama, J. Phys: Theo. and Appl. **3**, 9 (2019).
[19] R. K. Panda, R. Muduli, and D. Behera, J. Alloys Comp. **634**, 239 (2015).
[20] K. Rana, P. Thakur, P. Sharma, M. Tomar, V. Gupta, and A. Thakur, Ceram. Int. **41**, 4492 (2015).
[21] R. Safi, A. Ghasemi, R. Shoja-Razavi, and M. Tavousi, J. Magn. Magn. Mater. **396**, 288 (2015).
[22] S. Amiri and H. Shokrollahi, J. Magn. Magn. Mater. **345**, 18 (2013).
[23] R. D. Waldron, Infrared spectra of ferrites, Physical Review **99**, 1727 (1955).